Calibration of EUV-2D Photoresist Simulation Parameters for Accurate Predictive Modelling

Stewart A. Robertson[a], Patrick P. Naulleau[b], Donna J. O'Connell[c], Kevin McDonald[c], Todd Delano[a], Kenneth A. Goldberg[b], Steven G. Hansen[d], Kirk W. Brown[a] and Robert L. Brainard[a]

[a]Shipley Company L.L.C., 455 Forest Street, Marlborough, MA 01752
[b]Lawrence Berkeley National Laboratory, Berkeley CA 94720
[c]Sandia National Labs, P.O. Box 969, M/S 9409; Livermore, CA 94551
[d]ASML TDC , 8555 S.River Parkway, Tempe, AZ 85284

ABSTRACT

In this work simulation parameters are developed for Shipley EUV-2D photoresist under exposure at 13.4nm. Baseline parameter values are determined from theory and experiment. The simulation parameters were tuned from these values using a commercial automatic parameter optimization software to match simulation results to experimental lithographic data generated using the ETS Set-2 projection optics in the subfield exposure station (SES). In an attempt to maximise parameter accuracy the experimental data set used included 4 different feature sizes and known non-idealities of the exposure set-up were accounted for (mask errors, lens aberrations and metrology bias). The resulting model described the experimental data very well with only a low level of residual error.

Keywords: extreme ultraviolet lithography, lithography simulation, modelling parameter optimization

1. INTRODUCTION

Extreme ultraviolet (EUV) lithography is viewed as one of the leading candidates for the so-called *next generation lithography*, which will be utilized for the mass production of circuit features below the resolution limits of the refractive optical systems currently employed. Although encouraging experimental results[1-5] from early prototype tools have been presented, general access to the required exposure tools and masks is limited. Therefore lithography simulation is a key means of estimating the capabilities of proposed commercial lithographic tools and allows equipment vendors to determine the required tolerances for optical system aberrations and mask manufacture. The aerial image formed by EUV systems can be predicted accurately using rigorous electromagnetic propagation theory, accounting for such effects as optical element aberrations and mask topography. However, the final utility of EUV modelling depends upon the response of the photoresist to the presented aerial image. Although some work has been done on the calibration of a resist model for an EUV resist material, no comprehensive simulation parameters have been developed. In this work, a combination of experimental lithographic data and fundamental resist parameter measurements are used to produce a calibrated model for the Shipley EUV-2D photoresist.

2. EXPERIMENTAL EUV EXPOSURES

2.1 The Subfield Exposure Station

All the EUV exposure utilized in the work were performed on the Subfield Exposure Station (SES) at Lawrence Berkeley National Laboratory with the set-2 optic designed for the EUV LLC Engineering Test Stand (ETS). The SES system has a synchrotron based source and exposed a 100µm subfield at the wafer. Imaging is in a static mode utilizing

 © 2003 SPIE · 0277-786X/03/$15.00

standard reflection masks developed for the ETS. A full description of the SES is given by Naulleau *et al*.[1] The optic aberrations and flare terms of the set-2 optic have been characterized the by the Virtual National Lab (VNL) using a wavefront phasemap[6] (Shown in Figure 1). This analysis showed that the RMS error in the optic was in the order of 1/20 wavefront.

2.2 Experimental Conditions

The resist processing conditions and the optical configuration of the SES used during the experimental work is detailed in Table 1. The features studied were four sets of dense lines with nominal critical dimensions of 100nm, 90nm, 80nm and 70nm. Process windows were determined for each of the features utilizing a Focus-Exposure Matrix (FEM) with steps of 0.30 µm in focus and dose was varied from 5.73 to 8.89 mJ/cm^2 in 5% increments. SEM measurements of the mask showed that in each case the lines on the mask were oversized by approximately 5nm (wafer level). Critical dimension analysis of the printed images was made top down using a Leo 1560 SEM. The resulting Bossung plots are shown in Figures 2(a), 3(a), 4(a) and 5(a).

Parameter	Value
Objective NA	0.1
Illuminator σ	0.7
Substrate	Bare Si
Resist Thickness	120nm EUV-2D
Softbake	60s @ 140°C
PEB	90s @ 130°C
Develop	60s SSP MF LDD-26W

Table 1: Experimental process conditions.

3. BASELINE SIMULATION PARAMETERS

The lithography simulation package employed in this study is PROLITH v7.2.2 (KLA-Tencor, FINLE Division, Austin TX). In order to model a chemically amplified resist in this software one needs to define at least 30 material/process dependent input parameters (more depending upon the resist models chosen). These can be split into four broad categories; optical properties, acid generation efficiency, dissolution rate parameters and PEB kinetics. The resulting baseline parameters are detailed in Table 2.

3.1 Optical Parameters

Resist optical parameters (refractive index, Dill A and Dill B) cannot be measured at EUV wavelength (13.4nm) using the techniques standardly employed to characterize photoresists at longer wavelengths (157nm, 193nm, 248nm etc.). The optical parameters for the EUV-2D photoresist at 13.4nm were generated from theory using the web software available from the Centre of X-ray (CXRO)[7], which allows the resist's complex index of refraction to be calculated from knowledge of the materials elemental composition and the density of the dry spuncast film. The Dill parameters can be derived from the extinction coefficient (k), working on the assumption that the material exhibits negligible bleaching or darkening at the exposure wavelength upon exposure, i.e. Dill A (13.4nm) = 0.000 μm^{-1}.

3.2 Acid Generation Efficiency

Acid generation efficiency describes the amount of photo-generated acid that is produced within a photoresist for a given amount of incident energy. Szmanda *et al*.[8] described a method for determining this value by creating a series of photoresists with a varying molar ratio of photoacid generator to quencher base. The acid generation efficiency is calculated from the gradient of the plot of clearing dose against the PAG to quencher ratio. An accurate value for the acid

generation efficiency is obtained once corrections are made for the amount of incident energy actually coupled into the film and absorption within the film. In this instance, four resist formulations were made and clearing doses were determined on the SES exposure system.

3.3 PEB Kinetic Parameters

These parameters describe how the acid catalysed polymer deprotection reaction proceeds during the PEB. They include acid loss mechanisms, acid and base diffusion parameters in addition to the values that describe the deprotection reaction kinetics. Since EUV2D is an annealing, high activation energy photoresist, several reasonable assumptions can be made that simplify the resist model. These assumptions are i) All acid loss mechanisms can considered negligible ii) base diffusion is negligible and iii) the acid reaction order is unity. Due to the difficulties involved in exposing resist areas larger than 100μm, all the kinetic parameters were determined for the resist using 248nm exposures, i.e. a full standard resist model was made for the EUV-2D material using standard resist modelling techniques in a manner similar to that described by Kang *et al*.[9,10] This approach assumes that once a photoacid has been generated from a PAG molecule it diffuses and deprotects the polymer regardless of the original exposure wavelength.

3.4 Dissolution Rate Parameters

The dissolution rate equation parameters describe the relationship between deprotection level and the dissolution rate of the polymer in developer solution. Again these values were determined using 248nm exposure using standard techniques described previously.[9,10]

4. MODELING ASSUMPTIONS AND NON-IDEALITIES

4.1 Mask Modelling

With few exceptions, the majority of lithography simulation work undertaken to model the behaviour of contemporary lithography techniques (F_2, ArF, KrF, I-line and g-line) assumes that a mask can be represented by an infinitely thin plane, varying only in phase and transmission properties. This assumption is usually sufficient since the vertical dimensions of the physical mask topography (~100nm) are small relative to the imaging wavelength. However, in EUV lithography, the alternating stacks of Mo/Si used to make the EUV mirrors and the absorber layer can result in mask topography layers which are more than 30 times greater than the illumination wavelength. The resulting “thick” mask effects can result in asymmetry of focus effects. However, it has been noted that these mask “shadowing” effects are only significant when the illuminating radiation arrives at the mask significantly off normal incidence.[11] In practice, the effects can be ignored for low NA (< 0.20) cases. Consequently, the thin mask approximation is employed in this work, since the Set-2 ETS optic has 0.1NA.

Measurements of the mask showed that the absorber regions of the dense line structures studied in this work were uniformly oversized by 20nm (5nm at wafer scale). The correct, rather than nominal, mask dimensions were utilized in all simulations.

4.2 Flare

The level of stray light in the ETS Set-2 optic has been characterized at 20%.[12] Whilst this is a considerable improvement on the set-1 optic (48%), it is too high to be ignored. The impact of the stray light is accounted for in this work by the high frequency components of the phasemap information (which extends well beyond the typical 36 Zernike polynomial level). However, no additional D.C. flare term was included.

4.3 Metrology Offset

Previous work[13] has shown that the use of a metrology offset can be crucial in obtaining good resist modelling parameters. Historically, the correlation between simulation and cross-section has been good but some transformation of the simulated data has been required to replicate top-down measurements. The CD measurement offset represents a

simple but effective first order means of matching simulation to top-down measurements, though significantly more sophisticated approaches are under development.[14] In this instance top-down measurements are done at high voltage with gold coating and previous results have suggested negligible offset should be evident, however it is worth noting that the ~2 nm thick gold coat will offset the measured CD from the "real" CD. To this end the CD metrology offset will be allowed to float during the optimization process.

5. CALIBRATION PROCEDURE

The optimization of the parameters utilized the AUTOTUNE option of PROLITH which allows simulation parameters to be varied with defined limits to give the simulation input parameters which give the lowest reported residual error to the experimental dataset, which is reported in terms of a sigma value. The software allows a single set of resist parameters to be matched to several Focus-Exposure Matrices simultaneously,[15] in this case the four previously described. Obviously, there are a large number of input parameters which can be varied in the optimization, however the subset studied can be limited since the relative uncertainty in the baseline parameter measurement is generally known, and the impact each parameter has on the final result is generally known.

To this end the resist simulation parameters that were allowed to float were restricted to acid generation efficiency, PEB acid characteristic diffusion length, acid amplification constant (acid reaction order was constrained to unity), minimum dissolution rate, and developer contrast. Additionally, the CD metrology offset and the focus offset between experiment and simulation were also allowed to float. Table 2 details the optimized parameter set.

Although the optimization procedure should be completely automated, the large number of floating variables resulted in a significant amount of manual intervention to find the global minimum input parameter values

Parameter	Baseline Value	Optimized Value
Refractive Index	0.9765	0.9765
Dill A	0.0000 1/µm	0.0000 1/µm
Dill B	5.1851 1/µm	5.1851 1/µm
Acid Generation Efficiency	0.0883 mJ/cm^2	0.1053 mJ/cm^2
Thermal Decomposition	None	None
PEB Characteristic Diffusion Length	63.2 nm	37.8 nm
Diffusivity Variation	Constant	Constant
Room Temperature Diffusion Length	None	None
Amplification Reaction Order	1	1
PEB Amplification Constant	0.0781	0.1047
PEB Bulk Acid Loss	None	None
PEB Acid Evaporation	None	None
PEB Diffusion-Controlled Reaction Constant	119970	119970
Mack Model R_{max}	451.2 nm/s	451.2 nm/s
Mack Model R_{min}	0.1500 nm/s	0.0826 nm/s
Mack Model n	9.2	24.95
Mack Model M_{th}	0.55	0.55
CD Metrology Offset	0 nm	4 nm
Focus Offset	0.00 µm	-0.07 µm

Table 2: Baseline and optimized simulation parameters. Grey shading indicates the parameters allowed to float in the optimization process.

6. DISCUSSION OF RESULTS

The fully optimized simulations parameters returned a sigma value of 2.74 nm when all data points in all four FEMs were considered. This excellent level of agreement is illustrated in Figures 2 – 5, which show the experimental and simulated data side by side for each of the features of interest. In each case the Klarity PRODATA v1.3.2 (KLA-Tencor, FINLE Division, Austin TX) polynomial fit to the points is shown. Figure 6 compares the experimental and simulated process windows, as determined by PRODATA, for each of the four features. This figure clearly demonstrates the high quality of simulated results, as all errors in the process windows are below one step in both focus and exposure. It is interesting to note that the optimal CD metrology offset is 4nm, the theoretical CD shift induced by the gold sputtering on the sample. The "exactness" of the result is most likely coincidence, however, it shows that the optimized values are consistent with the known facts. All other parameter values are in the range one would typically expect for this type of resist formulation. It is worth noting that the impact of quencher base diffusion was investigated during this work. Whilst some level of quencher diffusion undoubtedly occurs within the resist during PEB, its inclusion in the simulation did not improve the quality of the simulation results.

7. CONCLUSIONS

A photoresist model has been developed for EUV-2D using a standard chemically amplified photoresist model which accurately predicts the performance of the resist material when exposed using EUV illumination. The simulations give excellent agreement with the experimental data used for model calibration. The good fit quality can be attributed, at least partially, to the careful inclusion of known, significant, non-idealities in the resist processing procedure.

ACKNOWLEDGMENTS

The authors would like to thank Matthew Weschler of FEI (Hillsboro, OR), for assistance in obtaining cross-sectional images, DARPA for partial funding of this work (Contract N66001-01-C-8069) and the EUV-LLC member companies (Intel, Motorola, AMD, IBM, Micron and Infineon)

REFERENCES

1. Naulleau, P. P., Goldberg, K. A., Anderson, E. H., Attwood, D., Batson, P., Bokor, J., Denham, P., Gullikson, E., Harteneck, B., Hoef, B., Jackson, K., Olynick D., Rekawa, S., Salmassi, F., Blaedel, K., Chapman, H., Hale, L., Soufli, R., Spiller, E., Sweeney, D., Taylor, J., Walton, C., Ray-Chaudhuri, A., O'Connell, D., Stulen, R., Tichenor, D., Gwyn, C.W., Yang, P-Y., and Zhang, G., "Static Microfield Printing at the Advanced Light Source with the ETS Set-2 Optic", SPIE Vol. 4688, *Emerging Lithographic Technologies VI*, pp. 64-71, 2002.

2. Tichenor, D. A., Replogle, W. C., Lee, S. H., Ballard, W. P., Leung, A. H., Kubiak, G. D., Klebanoff, L. E., Graham, S., Goldsmith, J. E. M., Jefferson, K. L., Wronosky, J. B., Smith, T. G., Johnson, T. A., Shields, H., Hale, L. C., Chapman, H. N., Taylor, J. S., Sweeney, D. W., Folta, J. A., Sommargren, G. E., Goldberg, K. A., Naulleau, P., Attwood, D. T., and Gullikson, E. M., "Performance upgrades in the EUV Engineering Test Stand", SPIE Vol. 4688, *Emerging Lithographic Technologies VI*, pp. 72-86, 2002.

3. Lee, S. H., Tichenor, D. A., Ballard, W. P., Bernardez, L. J. II, Goldsmith, J. E. M., Haney, S. J., Jefferson, K. L., Johnson, T. A., Leung, A. H., O'Connell, D., Replogle, W. C., Wronosky, J. B., Blaedel, K., Naulleau, P. P., Goldberg, K. A., Gullikson, E., Chapman, H., Wurm, S., Panning, E., Yan, P-Y, Zhang, G., Bjorkholm, J. E., Kubiak, G. D., Sweeney, D. W., Attwood, D., and Gwyn, C.W.," Lithographic Evaluation of the EUV Engineering Test Stand", SPIE Vol. 4688, *Emerging Lithographic Technologies VI*, pp. 266-276, 2002.

4. Cobb, J., Dentinger, P., Hunter, L., O'connell, D., Gallatin, G., Hinsberg, B., Houle, F., Sanchez, M., Domke, W-D., Wurm, S., Okoroyanwu, U., and Lee, S-H, " EUV Photoresist Performance from the VNL and the EUV LLC", ", SPIE Vol. 4688, *Emerging Lithographic Technologies VI*, pp. 412-420, 2002.

5. Hamamoto, K., Watanabe, T., Hada, H., Komano, H., Kishimura, S., Okazaki, S., and Kinoshita, H., "Fine Pattern Replication on 10-mm x 10-mm exposure area using ETS-1 laboratory tool in HIT", ", SPIE Vol. 4688, *Emerging Lithographic Technologies VI*, pp. 664-671, 2002.

6. Goldberg, K. A., Naulleau, P. P., Bokor, J., and Chapman, H., "Honing the Accuracy of Extreme Ultraviolet Optical System Testing: At-wavelength and visible-light measurements of the ETS Set-2 Projection Optic", SPIE Vol. 4688, *Emerging Lithographic Technologies VI*, pp. 329-337, 2002.

7. http://www-cxro.lbl.gov/optical_constants/getdb2.html

8. Szmanda, C. R., Kavanagh, R. J., Bohland, J. R., Cameron, J. F., Trefonas, P., Blacksmith, R. F., "Simple method for measuring acid generation quantum efficiency at 193 nm", SPIE Vol. 3678, *Advances in Resist Technology and Processing XVI*, pp. 857-866, 1999.

9. Kang, D., Pavelchek, E. K., and Swible-Keane, C., "Accuracy of Current Model Descriptions of a DUV Photoresist", SPIE Vol. 3678, *Advances in Resist Technology and Processing XVI,* pp. 877-890, 1999.

10. Kang, D., Robertson, S. A., and Pavelchek, E. K. "Simulation of 193-nm photoresists based on different polymer platforms", SPIE Vol. 4345, *Advances in Resist Technology and Processing XVIII,* pp. 936-944, 2001.

11. Krautschik, C., Ito, M., Nishiyama, I., and Otaki, K., "The Impact of the EUV Mask Phase Response on the Asymmetry of Bossung Curves as Predicted by Rigorous EUV Mask Simulations", SPIE Vol. 4343, *Emerging Lithographic Technologies V*, pp. 392-401, 2001.

12. Ballard, W. P., Tichenor, D. A., O'Connell, D. J., Bernardez, L., J. II, Lafon, R. E., Anderson, R. J., Leung, A. H., Williams, K., Haney, S. J., Perras, Y., Jefferson, K. L., Porter, T. L., Knight, D., Barr, P. K., Van De Vreugde, J. L., Campiotti, R. H., Zimmerman, M. D., Johnson, T. A., Klebanoff, L. E., Grunow, P. A., Graham, S., Buchenauer, D. A., and Replogle, W. C., "System and Process Learning in a Full-Field High-Power EUVL Alpha Tool", SPIE Vol. 5037, *Emerging Lithographic Technologies VII*, Paper 6, 2003.

13. Robertson, S. A., Kang, D., Tye, S. D., Hansen, S. G., Fumar-Pici, A., Chiou, T-B., Byers, J. D., Mack, C. A., Smith, M. D., "Calibration of ESCAP Resist Simulation Parameters from Consideration of Printed CD Pitch Bias, CD Measurement Offset and Wafer Thermal History", SPIE Vol. 4690, *Advances in Resist Technology and Processing XIX*, pp. 952-962, 2002.

14. Jones, R., Byers, J., and Conely, W., "Top Down versus Cross-Sectional SEM Metrology and its Impact on Lithography Simulation Calibration", SPIE Vol. 5038, *Metrology, Inspection, and Process Control for Microlithography XVII*, Paper 70, 2003.

15. Byers, J.D., Mack, C.A., Huang, R. and Jug, S., "Automatic calibration of lithography simulation parameters using multiple data sets", *MNE 2001*, Paper PH7, 2001

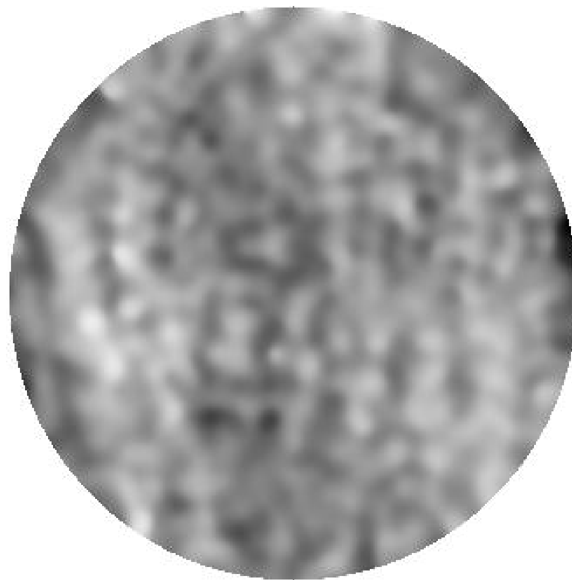

Figure 1: Phasemap for field point 22 of the ETS Set-2 optic. Lightest to darkest area represent phase change of -112° to +127°.

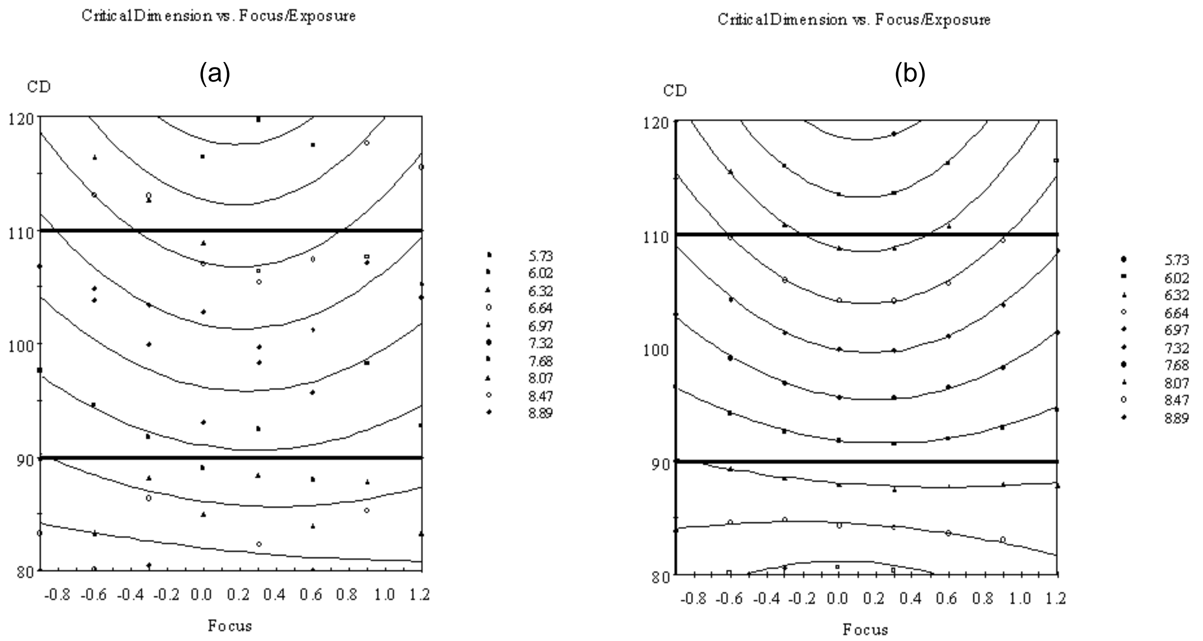

Figure 2: 100nm L/S Bossung plots for (a) experimental data (b) optimized simulation parameters.

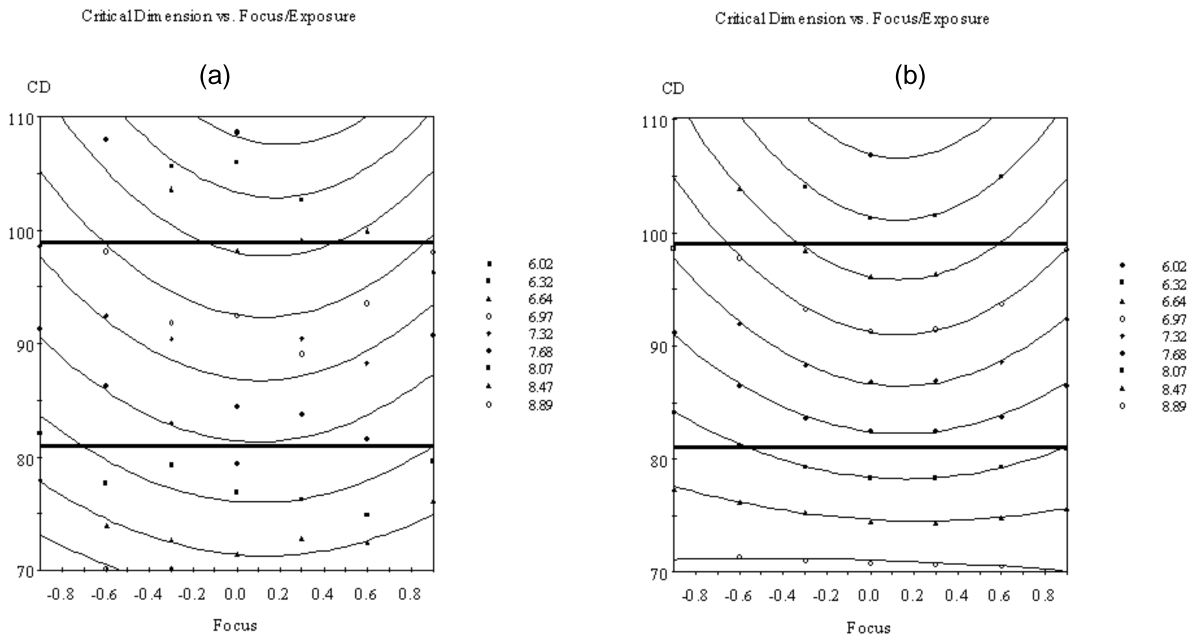

Figure 3: 90nm L/S Bossung plots for (a) experimental data (b) optimized simulation parameters.

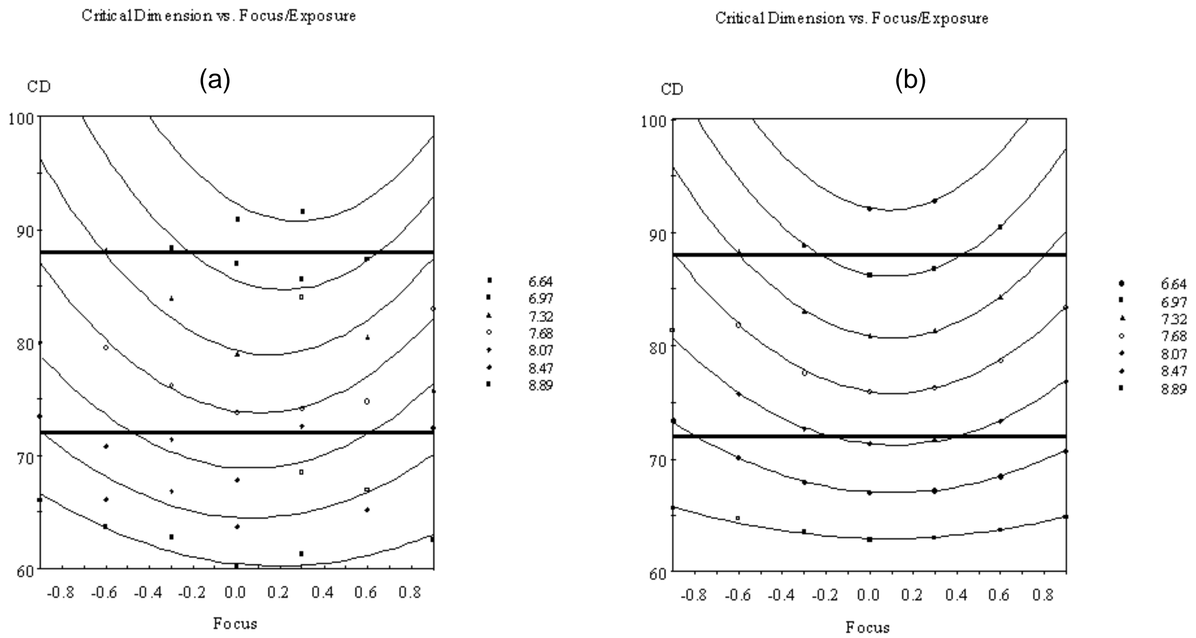

Figure 4: 80nm L/S Bossung plots for (a) experimental data (b) optimized simulation parameters.

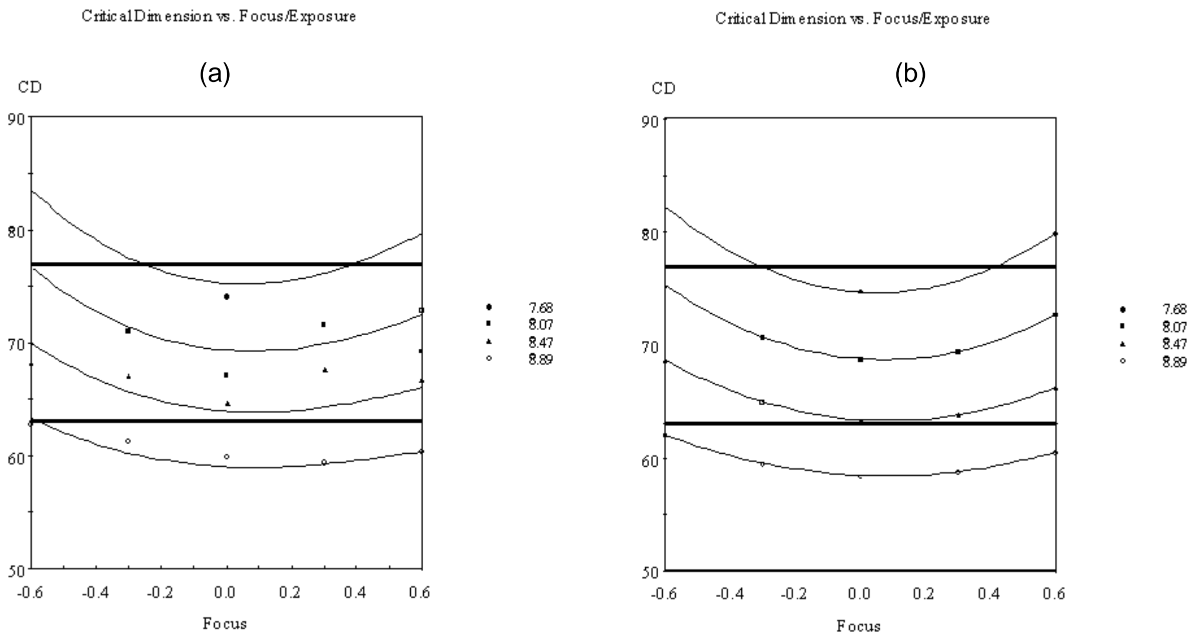

Figure 5: 70nm L/S Bossung plots for (a) experimental data (b) optimized simulation parameters.

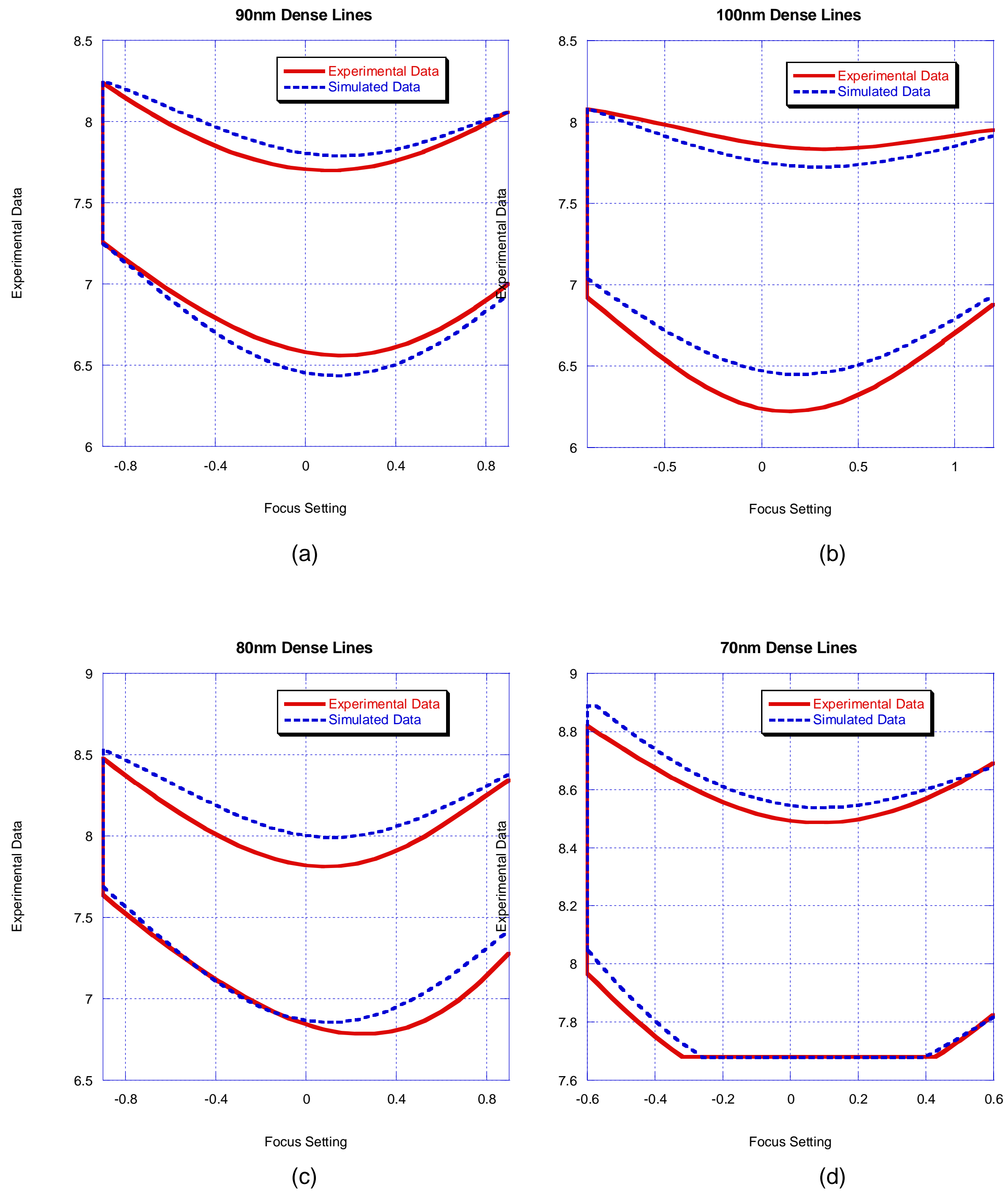

Figure 6: Process window comparison between experimental and optimized simulation parameters for (a) 100nm dense lines, (b) 90nm dense lines, (c) 80nm dense lines and (d) 70nm dense lines.